



# LUND UNIVERSITY

## Biofuel cell based on microscale nanostructured electrodes with inductive coupling to rat brain neurons.

Andoralov, Viktor; Falk, Magnus; Suyatin, Dmitry; Granmo, Marcus; Sotres, Javier; Ludwig, Roland; Popov, Vladimir O; Schouenborg, Jens; Blum, Zoltan; Shleev, Sergey

*Published in:*  
Scientific Reports

*DOI:*  
[10.1038/srep03270](https://doi.org/10.1038/srep03270)

2013

[Link to publication](#)

### *Citation for published version (APA):*

Andoralov, V., Falk, M., Suyatin, D., Granmo, M., Sotres, J., Ludwig, R., Popov, V. O., Schouenborg, J., Blum, Z., & Shleev, S. (2013). Biofuel cell based on microscale nanostructured electrodes with inductive coupling to rat brain neurons. *Scientific Reports*, 3(Nov 20), [3270]. <https://doi.org/10.1038/srep03270>

*Total number of authors:*  
10

### **General rights**

Unless other specific re-use rights are stated the following general rights apply:  
Copyright and moral rights for the publications made accessible in the public portal are retained by the authors and/or other copyright owners and it is a condition of accessing publications that users recognise and abide by the legal requirements associated with these rights.

- Users may download and print one copy of any publication from the public portal for the purpose of private study or research.
- You may not further distribute the material or use it for any profit-making activity or commercial gain
- You may freely distribute the URL identifying the publication in the public portal

Read more about Creative commons licenses: <https://creativecommons.org/licenses/>

### **Take down policy**

If you believe that this document breaches copyright please contact us providing details, and we will remove access to the work immediately and investigate your claim.

LUND UNIVERSITY

PO Box 117  
221 00 Lund  
+46 46-222 00 00



OPEN

SUBJECT AREAS:

CHEMICAL PHYSICS

NEUROSCIENCE

IMMOBILIZED ENZYMES

BIOANALYTICAL CHEMISTRY

# Biofuel Cell Based on Microscale Nanostructured Electrodes with Inductive Coupling to Rat Brain Neurons

Viktor Andoralov<sup>1\*</sup>, Magnus Falk<sup>1\*</sup>, Dmitry B. Suyatin<sup>2,3</sup>, Marcus Granmo<sup>2</sup>, Javier Sotres<sup>1</sup>, Roland Ludwig<sup>4</sup>, Vladimir O. Popov<sup>5,6</sup>, Jens Schouenborg<sup>2</sup>, Zoltan Blum<sup>1</sup> & Sergey Shleev<sup>1,6</sup>

Received  
31 May 2013

Accepted  
31 October 2013

Published  
20 November 2013

Correspondence and requests for materials should be addressed to S.S. (sergey.shleev@mah.se)

\* These authors contributed equally to this work.

<sup>1</sup>Biomedical Sciences, Health & Society, Malmö University, 205 06 Malmö, Sweden, <sup>2</sup>Neuronano Research Center, Medical Faculty, Lund University, 221 00 Lund, Sweden, <sup>3</sup>Division of Solid State Physics and The Nanometer Structure Consortium (nmC@LU), Lund University, 221 00 Lund, Sweden, <sup>4</sup>Food Biotechnology Laboratory, Department of Food Sciences and Technology, BOKU-University of Natural Resources and Life Sciences, 1190 Vienna, Austria, <sup>5</sup>Kurchatov NBIC Centre, National Research Centre “Kurchatov Institute”, 123182 Moscow, Russia, <sup>6</sup>A.N. Bach Institute of Biochemistry, 119 071 Moscow, Russia.

Miniature, self-contained biodevices powered by biofuel cells may enable a new generation of implantable, wireless, minimally invasive neural interfaces for neurophysiological *in vivo* studies and for clinical applications. Here we report on the fabrication of a direct electron transfer based glucose/oxygen enzymatic fuel cell (EFC) from genuinely three-dimensional (3D) nanostructured microscale gold electrodes, modified with suitable biocatalysts. We show that the process underlying the simple fabrication method of 3D nanostructured electrodes is based on an electrochemically driven transformation of physically deposited gold nanoparticles. We experimentally demonstrate that mediator-, cofactor-, and membrane-less EFCs do operate in cerebrospinal fluid and in the brain of a rat, producing amounts of electrical power sufficient to drive a self-contained biodevice, *viz.*  $7 \mu\text{W cm}^{-2}$  *in vitro* and  $2 \mu\text{W cm}^{-2}$  *in vivo* at an operating voltage of 0.4 V. Last but not least, we also demonstrate an inductive coupling between 3D nanobioelectrodes and living neurons.

Research on neural interfaces has the potential to revolutionise our understanding of fundamental neural mechanisms and is likely to engender new opportunities for clinical diagnosis and therapy<sup>1–3</sup>. Microscale autonomous, *i.e.* self-powered and wirelessly communicating, biodevices constitute a new generation of implantable neural interfaces. Such biodevices enable minimally intrusive, *in vivo* neurophysiological studies and therapies on a sub-cellular level. The overall dimensions and self-sufficiency of the biodevices significantly improve the implantable properties, thus enabling an unprecedented level of biodevice biocompatibility, reliability, and longevity due to complete physical and electrical decoupling from external devices. Indeed, such self-contained biodevices may reveal the full potential of nanostructure based neuronal interfaces for *in vivo* applications<sup>4,5</sup>.

Wireless self-powered neural biodevices could for instance carry a probe for neuronal signal detection connected to a nano-amplifier and a nano-transmitter; all of which could be powered by a membrane- and mediator-less enzymatic fuel cell (EFC, Fig. 1). The functionality of these discrete nanoelectronic elements has already been demonstrated<sup>6–8</sup>. Moreover, *in vivo* studies of nanowire based neuronal electrodes have recently been performed<sup>9</sup>. Our work details the last element needed to design autonomous microscale biodevices, *viz.* an electric power source, specifically, a non-toxic and miniature EFC, capable of *in vivo* operation.

EFCs belong to a broad family of biofuel cells, which directly convert chemical energy into electric energy using biological catalysts, *e.g.* redox enzymes or even whole living cells<sup>10,11</sup>. Glucose/oxygen EFCs should provide a reliable source of electric energy for brain-device interfaces utilising the readily available biofuel, *e.g.* glucose, and biooxidant, *e.g.* molecular oxygen (O<sub>2</sub>), tapping into the same energy source as the biological entities of the brain. Recent calculations have demonstrated that the natural recirculation of the cerebrospinal fluid (CSF) in humans permits glucose energy harvesting at a rate of at least 1 mW, with no adverse physiological effects<sup>12</sup>. This suggests that EFCs can be used as a power source for minimally invasive wireless and self-powered biodevices in the brain. A few reports only exist on voltammetric studies of fully implantable EFCs operating *in vivo* in vertebrates<sup>13,14</sup> including rats<sup>15,16</sup>. All of these EFCs were macroscale, substantially limiting their practical application to act as an

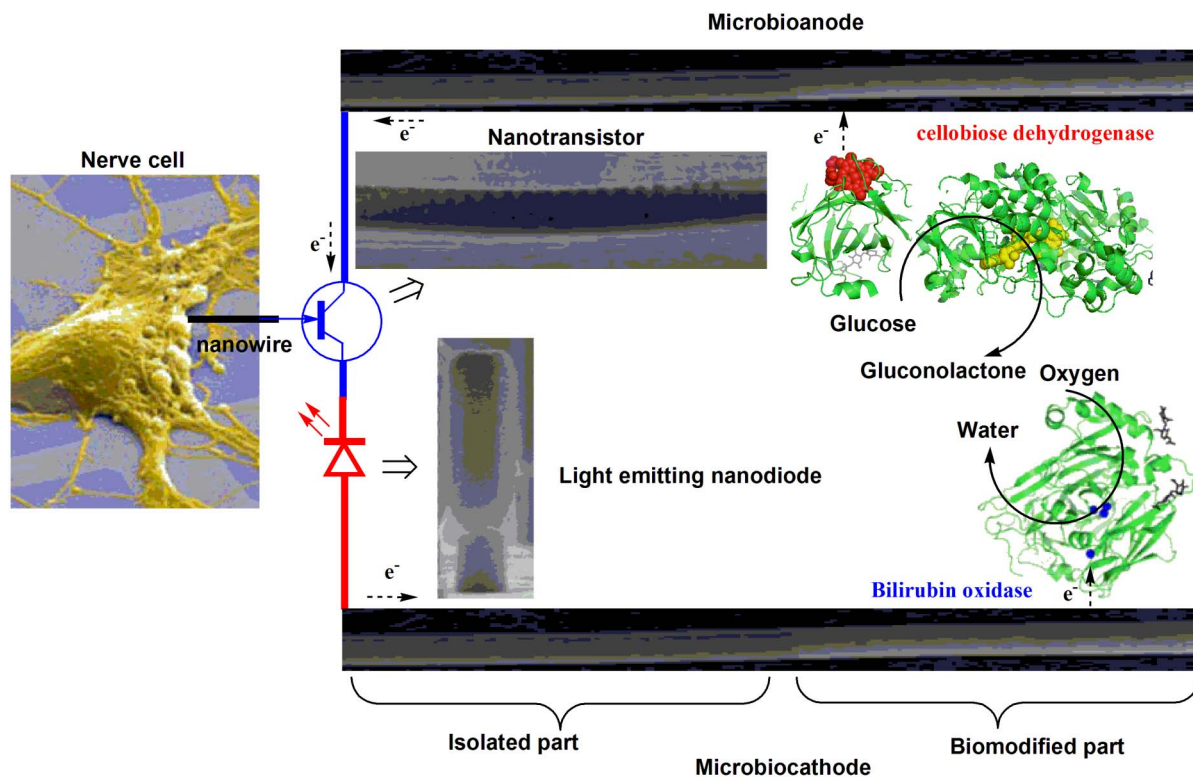


**Figure 1 | Minute autonomous biodevice for minimally invasive neuron interfacing.** Conceptual scheme of a wireless, self-powered biodevice for detection of neuronal signals which enables *in vivo* neurophysiological studies on a sub-cellular level with minimal intrusion and leads to a new generation of brain device interfaces. The images of a light emitting nanodiode, a nanotransistor, and a single neuron were adopted from Ref. 6, 8, 56. The structure of BOx was visualised based on the know crystal structure (PDB 2XLL) and CDH was designed using the cytochrome and the FAD domains of *Phanerochaete chrysosporium* cellobiose dehydrogenase (PDB 1D7D and 1NAA), respectively.

electric power source for miniature self-contained biodevices. Below we detail a microscale glucose/ $O_2$  EFC operating *in vivo* in a rat brain, following our earlier reports<sup>17–19</sup>.

One way to design EFCs for possible implantable applications is to immobilise glucose oxidising and oxygen reducing enzymes on nanostructured electrode surfaces to create an efficient bioanode and biocathode, respectively<sup>20,21</sup>. By electrically connecting the enzymes directly to the electrode, *i.e.* relying on direct electron transfer (DET), the usage of separator membranes and potentially toxic mediators can be avoided<sup>22</sup>. Accordingly, several membrane-, cofactor-, and mediator-less carbohydrate/oxygen EFCs have been reported in the literature<sup>23–26</sup>, and the design principle simplifies the setup and is pertinent to miniaturisation<sup>27</sup>.

Recently, a simple fabrication method for three-dimensional (3D) nanostructured electrodes, based on gold nanoparticles (AuNPs) was reported<sup>28</sup>. These electrodes have already been used to create micro- and macroscale biocathodes, bioanodes, and even complete EFCs<sup>17,22,26,27,29,30</sup>. However, there was no understanding of the process underlying the 3D nanostructure formation, and consequently the potential of this process was not fully appreciated. Here we show that the 3D nanostructure formation is due to an electrochemical transformation of the AuNPs deposited on Au electrodes, changing the surface morphology. The process is very simple and potentially applicable for formation of complex nanostructures from different materials and for a wide range of applications.

We use the process to construct microscale 3D nanostructured Au electrodes, increasing the geometric surface area a hundred times compared to unmodified electrodes (*i.e.* without AuNPs). The electrode morphology and electrical properties were characterised with electrochemical impedance (EI) spectroscopy and cyclic voltammetry (CV) and the data thus gathered correlated with the results from atomic force microscopy (AFM) and scanning electron microscopy

(SEM). In this way we show that the increased geometric area is due to 3D Au nanostructure formation and the electrodes were used to design high-performance, microscale glucose/oxygen EFCs. For the modification of the nanostructured electrodes thoroughly characterised anodic and cathodic bioelements were used.

A scheme of the EFC implemented in this study is shown in Fig. 1, where a glucose oxidising enzyme, cellobiose dehydrogenase (CDH), and an oxygen-reducing enzyme, bilirubin oxidase (BOx), are immobilised and directly wired to 3D microscale electrodes, resulting in a microbioanode and a microbiocathode, respectively. Glucose is oxidised to gluconolactone at the bioanode, transferring electrons to the electrode. At the biocathode electrons are transferred from the electrode to the enzyme, which reduces oxygen to water. By combining the microscale biocathode and bioanode, a miniature electric power generating EFC is realised. We experimentally prove that mediator- and membrane-less, microscale EFCs do generate electrical energy sufficient for a self-contained biodevice operating in CSF and in the rat brain. In addition, we also demonstrate that 3D microscale nanostructured electrodes establish well-pronounced inductive coupling with neurons in the brain, which is not only scientifically significant, but also permits active interactions, increasing the scope of implantable neural interfaces beyond that of passive monitoring.

## Results

**Fabrication and investigation of 3D nanostructured gold micro-electrodes.** To understand the formation process of 3D nanostructures and to firmly establish the structural features obtained, we performed detailed characterisation of the initially used AuNPs and 3D AuNPs based electrodes, as described below.

The size of the original AuNPs was determined by AFM; imaging of discrete NPs adsorbed on poly-lysine(PL)-coated mica surfaces



(Fig. 2a and 2b) indicated an average NP height of  $16.7 \pm 3.2$  nm (Fig. 2a, insert).

Microelectrodes coated with AuNPs were also imaged by AFM, before (Figs. 2c and 2d) and after (Figs. 2e and 2f) electrochemical treatment in 0.5 M  $\text{H}_2\text{SO}_4$  using CV, a common procedure for cleaning Au surfaces, and also widely used to estimate the real surface area of Au electrodes<sup>31</sup>. It can be seen that the AuNPs modified surface undergoes a major transformation during the  $\text{H}_2\text{SO}_4$  treatment, signified by a difference in the surface morphology. However, it was difficult to quantify the size of the transformed AuNPs, due to lack of a zero-height reference, but it was nonetheless clear that sizes increased with the electrochemical treatment, probably as a consequence of an aggregation process.

To obtain quantitative data of the features formed during the assembly of the 3D microscale electrodes, SEM studies were also

performed. The images in Fig. 3a, b, c were recorded after electrochemical cleaning of AuNP modified Au microwires in 0.5 M  $\text{H}_2\text{SO}_4$ , whereas Fig. 3d corresponds to the original AuNPs. On the modified side the average grain size was  $36 \text{ nm} \pm 12 \text{ nm}$ , whereas the average feature size was as high as  $77 \text{ nm} \pm 22 \text{ nm}$ . For comparison, in Fig. 3d the original nanoparticles can be seen, and in agreement with AFM data (cf. Figs. 2a and 3d) the average AuNP size used for modification was measured to be only  $17 \text{ nm} \pm 5 \text{ nm}$ .

In Fig. 3a the border between the AuNPs modified and bare Au microwire surface can be seen. It was observed (cf. Fig. 3b and 3c) that the particles merge into similar aggregates in the bulk, as well as on the border of the 3D nanostructured Au material, where the AuNPs coverage was limited to just a few monolayers. We conclude that the electrochemical treatment in  $\text{H}_2\text{SO}_4$  transforms the particles into a porous 3D nanostructured Au surface with an average grain size of

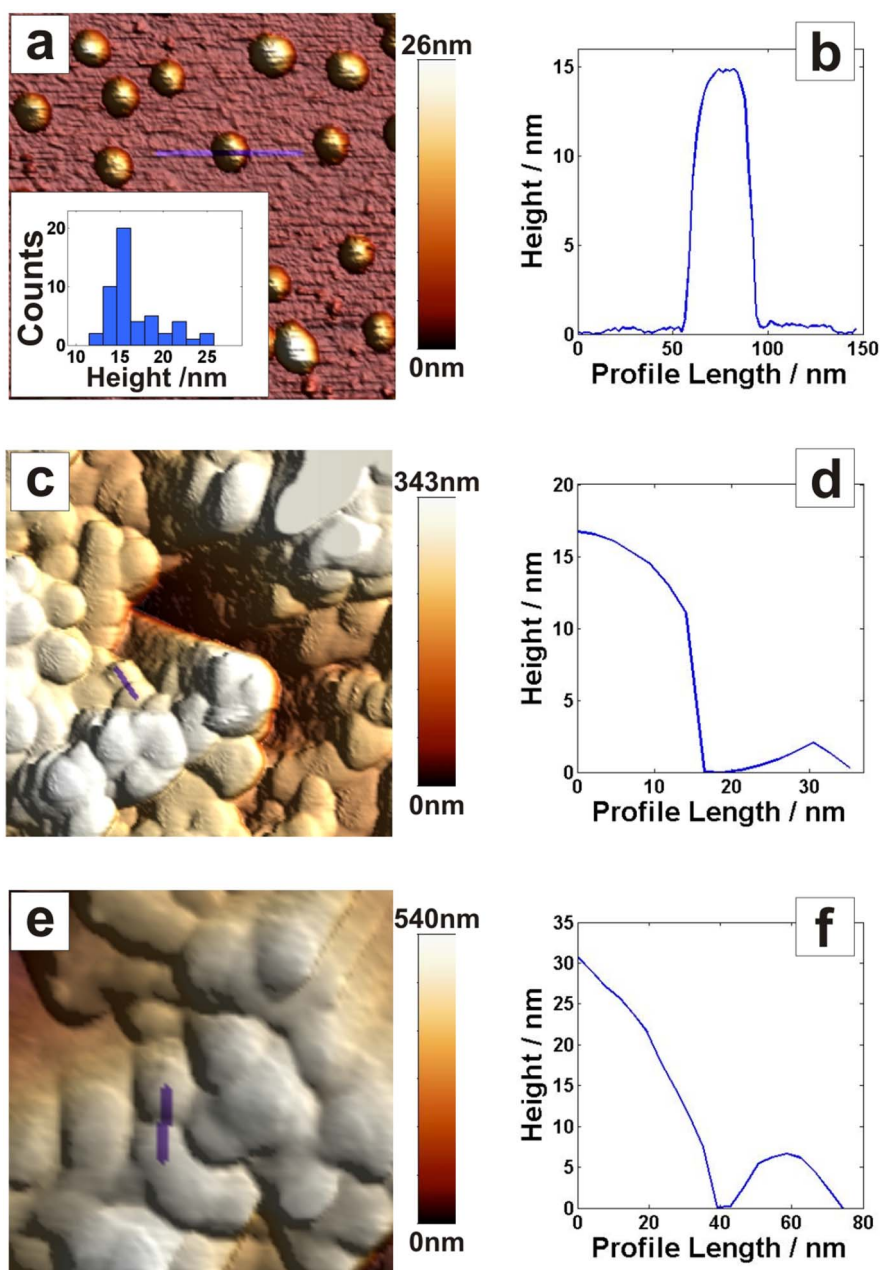


**Figure 2 | Atomic force microscopy studies of AuNPs and 3D nanostructured electrodes.** Images and corresponding height profiles of (a, b) AuNPs on a poly-lysine-coated mica surface, (c, d) microelectrode coated with AuNPs, (e, f) the microelectrode from panels c and d, after electrochemical cleaning. Scan areas for all images were  $400 \text{ nm} \times 400 \text{ nm}$ . Note that the height measured with AFM represents the diameter of the NPs; the width does not represent the diameter due to tip dilation effects<sup>57</sup>.



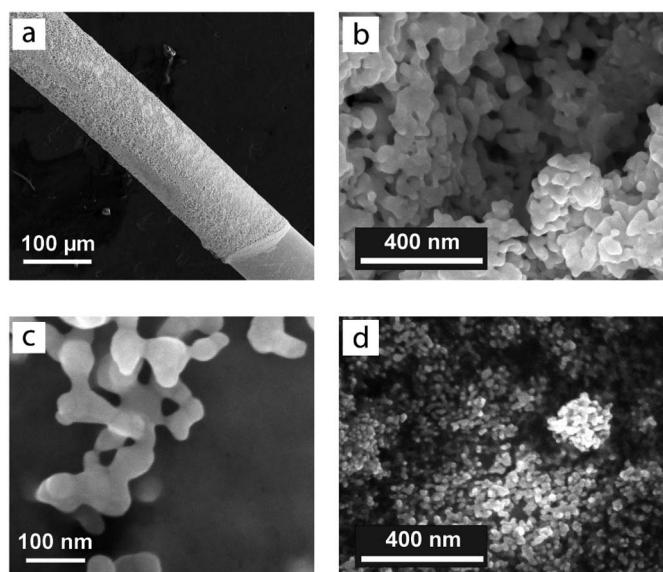


**Figure 3 | Scanning electron microscopy images of AuNPs modified microelectrodes.** (a) Low magnification image of the AuNPs modified Au microwire: the microwire geometry and the AuNP coating border can be seen in the lower right corner. (b) High magnification SEM image in the middle of the electrode in panel a. (c) High magnification SEM image of the border of the electrode in panel a. The images in panels a, b, and c were taken after the electrode modification with AuNPs and treatment in 0.5 M  $H_2SO_4$ . (d) SEM image of a reference sample covered with AuNPs identical to those used for the construction of nanobiostructures, the original nanoparticle shape can be clearly seen.

approximately 40 nm and an average feature size of approximately 80 nm, and since the border as well as the bulk show similar features, the transformation is independent of the AuNP layer thickness when a few monolayers of AuNPs up to thicker layers are employed.

In conclusion, genuinely 3D, electrically conducting microscale electrodes were fabricated by immobilising AuNPs on Au microwires, followed by electrochemical treatment of the electrodes. The AuNPs modified microelectrodes were further characterised electrochemically (Fig. 4) in a custom-built electrochemical setup for microelectrode characterisation in small volumes of physiological fluids (Fig. 4a). Increasing the amount of AuNPs on the electrode decreases the charge transfer resistance, due to the increased surface area with increased amount of AuNPs (Fig. 4b). Impedance plots measured for Au microwires modified with different amounts of AuNPs are shown in Fig. 4c. The impedance can be described using a circuit with resistance of charge transfer and open circuit Warburg impedance (inset Fig. 4c and d). The system (Au/AuNPs) displays a leakage current (charge transfer resistance) connected to oxygen reduction on the unmodified AuNPs surface. This is highly dependent on the potential of the electrode and the amount of AuNPs (Fig. 4c and d).

**Bioelements purification and characterisation.** To design efficient and stable microbioanodes and microbiocathodes *Corynascus thermophilus cellobiose dehydrogenase* (CtCDH) and *Myrothecium verrucaria* bilirubin oxidase (MvBOx) were deployed as anodic and cathodic biocatalysts, respectively. These enzymes have already been exploited in our previous work to fabricate DET based membraneless glucose/oxygen EFCs operating in plain glucose containing buffers, as well as complex human physiological fluids, such as blood, plasma, serum, saliva, and tears<sup>22,23,26,27</sup>. However, detailed biochemical and kinetic characterisation of the redox enzymes was not done, leaving questions regarding the reliability and reproducibility of the results unanswered. Thus, to address these questions, both bioelements were isolated, purified on a preparative scale, and

investigated in detail as described in SI (section 1 of Supplementary Information (SI), Figs. S1–S6, Tables S1–S2).

Concentrated high purity enzyme preparations in weak buffers (10–20 mM) were used for the construction of EFCs. For proper enzyme immobilisation on the electrode surface, the ionic strength, pH, and buffer composition were carefully controlled. The pH dependent catalytic activity of both biocatalysts used for EFC construction was obtained both in homogeneous solution and in the adsorbed state for biocatalytic and bioelectrocatalytic reactions. Obviously, the enzymes need to retain high activity within the EFC operational pH range (Supplementary Figs. S2 and S5).

The pH of the brain interstitial fluid (ISF) has been determined to be about 7.3, with pH values down to 7.1 at the centre of brain slices<sup>32</sup>. In the most extreme cases with severe ischemia or tissue hypoxia, the pH can drop to 6.0<sup>33</sup>. Accordingly, the activity of MvBOx and CtCDH was monitored in a wide pH range, when enzymes were immobilised on AuNPs modified electrodes, and compared to homogeneous reactions using different enzyme substrates, resulting in two different mechanisms of intramolecular electron transfer in the case of CDH<sup>34</sup> or different driving forces during homogeneous reactions catalysed by BOx<sup>35</sup>.

Briefly (all details can be found in SI), the results, as summarised in Fig. 5, indicate a good correlation between homogeneous and heterogeneous processes; the usual physiological pH range of ISF is highlighted in Fig. 5. In this region both enzymes retain at least 75% of their maximum activity. However, as the pH decreases the activity of CtCDH is significantly lowered, but about 50% of the activity remains even at pH 6.0.

**Fabrication and electrochemical study of biomodified 3D microscale Au electrodes.** Biomodification procedures of the 3D Au microelectrodes were conducted following a previously developed procedure for macroscale AuNPs modified electrodes<sup>26</sup>, adapted to microscale electrodes<sup>27</sup>.

Detailed electrochemical investigations of microbioanodes and microbiocathodes were performed in carbohydrate containing buffers and rat CSF. Chemical compounds are quite freely exchanged between CSF and ISF, making the composition of the ISF highly influenced by the CSF<sup>36</sup>. The amount of glucose in the CSF correlates with the concentration of glucose in blood, containing roughly two thirds of the blood amount, with a normal range of 2.5–4.5 mM<sup>37</sup>.

Linear sweep voltammograms (LSVs) of microbioanodes and microbiocathodes operating in different fluids are shown in Fig. 6a, b with a variation in the onset potential of  $\pm 5$  mV and maximum current outputs of  $\pm 12\%$ . For bioanodes, increasing the glucose concentration naturally increases the current generated by the anode (*cf.* curves 2–4 in Fig. 6a).

Compared to CSF, quite similar current levels are obtained in buffer solutions containing 2.5 mM glucose, (*cf.* curve 1 and 3, Fig. 6a). Contrary to bioanodes, the biocathode performance was essentially unaffected by the amount of glucose, but a large difference in both onset potential and current generated was observed between buffer and CSF (*cf.* curves 1 and 2, Fig. 6b). Most likely, the observed reduced performance of the EFCs in CSF is due to electrocatalytic oxidation (*i.e.* side reactions) of some other compounds present in this complex fluid (*e.g.* ascorbate, which is present at significant concentrations,  $\sim 160$   $\mu M$  compared to  $\sim 40$   $\mu M$  in blood<sup>38</sup>), catalysed by the underlying supporting material (*vide infra*); *e.g.* AuNPs are known to efficiently catalyse electrooxidation of different substrates including biofuels of EFCs<sup>39–41</sup>.

In addition to the voltamperometric studies, impedance measurements were performed to further investigate the influence of the supporting material on (bio)electrocatalytic reactions. For this purpose both unmodified and AuNPs-modified Au microwires were investigated in CSF (Fig. 6c–6f). The spectrum for a system consisting of two unmodified Au microelectrodes, displays a low charge transfer

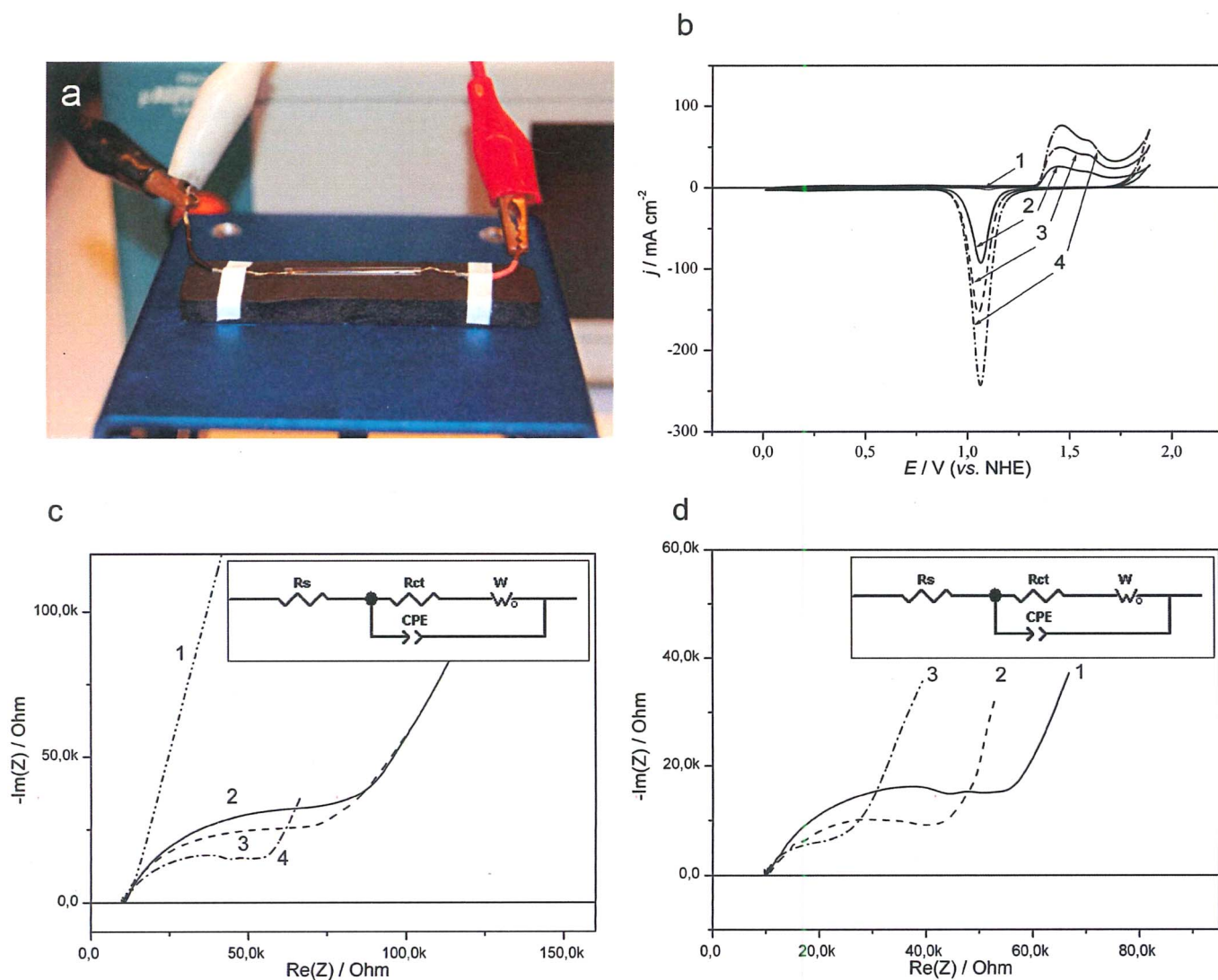


**Figure 4 | Electrochemical characterisation of AuNPs modified microelectrodes.** (a) Image showing the electrochemical setup for characterisation of microelectrodes. (b) Cyclic voltammograms, (c) Nyquist plots for Au microwires with different amount of AuNPs: 0  $\mu\text{L}$  (1), 3  $\mu\text{L}$  (2), 6  $\mu\text{L}$  (3), 12  $\mu\text{L}$  (4). (d) Nyquist plots at different potentials:  $-50\text{ mV}$  (1),  $-100\text{ mV}$  (2),  $-150\text{ mV}$  (3). Inset (c,d): Equivalent circuit  $R_s$  – solution resistance,  $W$  – Warburg impedance,  $R_{ct}$  – charge transfer resistance,  $CPE_{p1}$  – constant phase element. Conditions:  $0.5\text{ M H}_2\text{SO}_4$ ,  $100\text{ mV s}^{-1}$  (b);  $50\text{ mM PBS pH } 7.4$ ,  $-50\text{ mV}$  (c)  $50\text{ mM PBS pH } 7.4$ ,  $12\text{ }\mu\text{L}$  of AuNPs (d).

resistance and quite low total capacitance. For modified electrodes, one element in the high frequency region can be described by two parallel R-CPE circuits, corresponding to Faradaic processes, e.g. oxidation of interfering compounds present in CSF. Many different biocompounds that can be electrooxidised on the Au nanostructured surface are present in both ISF and CSF, e.g. antioxidants such as ascorbate, glutathione, uric acid, and neurotransmitters such as dopamine, serotonin and epinephrine<sup>42,43</sup>. These electrooxidative processes are much faster compared to the  $\text{O}_2$  reduction reaction occurring on the same electrode (cf. Fig. 4 and Fig. 6c–6f). The capacitance of 3D electrodes is 100 times higher compared to unmodified ones. Note that after the modification with both self-assembled monolayers and enzymes, the capacitance of 3D electrodes is insignificantly reduced (vide supra; Fig. 8c). Nevertheless, impedance studies also confirm the possibility of efficient non-enzymatic electrooxidation of biomolecules present in CSF by 3D Au microelectrodes.

**Experimental evaluation of the performance of miniature glucose/oxygen *in vitro* and *in vivo*.** *In vitro* measurements with CSF were performed using the microcell developed (Fig. 4a; vide supra), whereas the experimental setup used for *in vivo* studies can be seen in Fig. 7.

EFCs were investigated by connecting the bioanode (*CtCDH*/AuNP/Au) as a working electrode and the biocathode (*MvBOx*/AuNP/Au) as a combined reference and counter electrode. Steady-state measurements were performed by connecting calibrated resistors and measuring the voltage after the equilibration of the system, which was monitored by observing the stabilisation of the measured voltage. When the EFC was operated *in vitro*, open circuit voltages (OCVs) of  $0.65 \pm 0.03\text{ V}$  and  $0.57 \pm 0.01\text{ V}$  were obtained in glucose containing buffers and CSF, respectively, averaging from five different EFCs. The observed reduction in voltage of  $0.08\text{ V}$ , when the EFCs operated in CSF, was expected due to the drop in the onset potential of micro-biocathodes (Fig. 6b; vide supra). When the EFC was implanted in the brain of a rat, OCV values of  $0.54 \pm 0.03\text{ V}$  were registered, i.e. very close to the OCV obtained in CSF, confirming that ISF and CSF have similar compositions<sup>36,44,45</sup>. During some implantation procedures a localised surface bleeding occurred (cf. Fig. 7a and 7b). However, no difference in the performance of EFCs was observed (vide infra), whether a localised bleeding occurred during implantation or not.

It is important to emphasise that no changes in the voltage was registered, when several EFCs were connected in series in the brain. Thus, the operating voltage of a single EFC is a crucial parameter

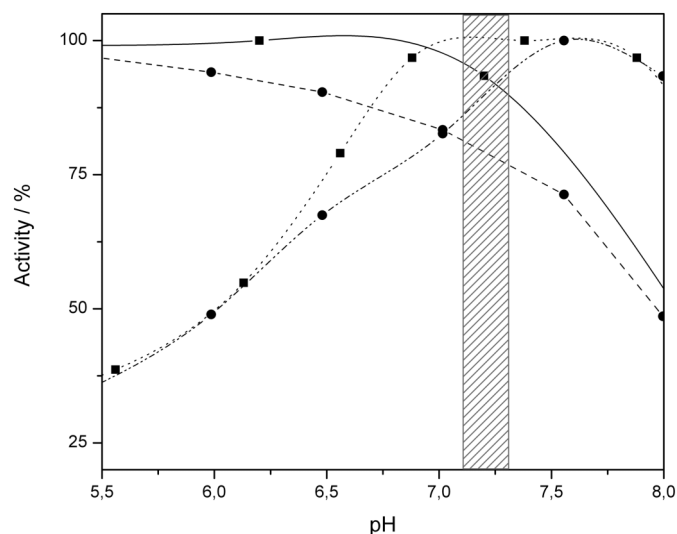


**Figure 5 | Activity of *Corynascus thermophilus* cellobiose dehydrogenase and *Myrothecium verrucaria* bilirubin oxidase at different pH values.** Activity *MvBOx* in solution with  $K_4[Fe(CN)_6]$  as the substrate (solid line, boxes) and immobilised on a RDE (dashed line, circles), as well as *CcDH* in solution with cytochrome *c* as the substrate (dotted line, boxes) and immobilised on a RDE (dash-dotted line, circles), with the pH region 7.1–7.3 highlighted. The rotation rate of the RDE was 2000 rpm.

when designing practically applicable power sources for implantable electronic biodevices.

Typical power profiles of EFCs operating both *in vitro* and *in vivo* are compared in Fig. 8a. A maximum power density of around  $4 \mu W cm^{-2}$ , ranging between  $\sim 3.2$ – $4.0 \mu W cm^{-2}$  at 0.4 V was generated by the EFC in a 2.5 mM glucose containing buffer and over  $7 \mu W cm^{-2}$  at a similar voltage in CSF, ranging between  $\sim 6.3$ – $7.2 \mu W cm^{-2}$ . In the brain, the maximum power density dropped to  $2 \mu W cm^{-2}$ , ranging between  $\sim 1.3$ – $2.1 \mu W cm^{-2}$  at a voltage of 0.4 V. Since no significant differences were observed, when actual steady-state measurements were used to evaluate the performance of EFCs, compared to the widely used LSVs measurements at low scan rates, the results presented in Fig. 8a were obtained under equilibrium conditions. Thus, one can easily re-plot the data based on a well-known and very simple equation, *viz.* power = voltage  $\times$  current.

The high power density and the different appearance of the power density profiles of EFCs operating in CSF compared to buffer solutions (*cf.* curves 1 and 2 in Fig. 8a) were obtained due to the combination of bioelectrocatalytic and electrocatalytic processes occurring on microbioanodes in the complex physiological fluid. Since significant power was generated when no enzyme was present on the anode, the electrooxidation of CSF on nanostructured microEFCs is most likely triggered by the supporting material (see details in section 3 of SI, Fig. S8)<sup>39,41</sup>. Thus, in addition to bioelectrooxidation of glucose, electrooxidation of antioxidants and neurotransmitters resulted in significant increase of power densities generated by EFCs at low voltages, *i.e.* in the 0.1 V–0.5 V range (curve 2 in Fig. 8a).

Operational stability tests of EFCs *in vivo* in the brain, as well as *in vitro* using buffer solutions and CSF, were performed by applying a constant load of 35.86 M $\Omega$ , and monitoring the voltage drop. The resistance value was chosen to perform stability tests in the appropriate way, *i.e.* at the maximal performance of EFCs, when biodevices deliver maximal power: *ca.* 11 nA at 0.4 V, or  $2 \mu W cm^{-2}$ . Typical stability curves of EFCs operating in buffer, CSF, and brain tissue are presented in Fig. 8b. A reduction in voltage of roughly 50% after 2 h of continuous EFC operation in the brain was observed (Fig. 8b,

curve 3). At the time marked with an arrow in Fig. 8b, the electrodes were carefully displaced 0.1–0.2 mm vertically while inserted in the brain. This resulted in the voltage returning to the original value, which indicated that the observed drop in performance is not related to bioelements deactivation. Most likely the diffusion properties of the brain tissue limit the power of the EFC. When no load was applied to the EFC the OCV remained unchanged for at least 3 hours. In buffer solutions and CSF, EFCs displayed excellent stability with over 90% and 85% of the initial voltage remaining after 2 h of continuous operation, respectively (curves 1 and 2 in Fig. 8b). It is worthwhile to mention a significant increase in power density (from 2 up to  $4 \mu W cm^{-2}$ ), when the cortical depth for implanted EFCs was decreased from 2 mm to 1 mm.

In additional experiments OCVs of implanted EFCs after an injection of a lethal dose of barbiturate was continuously monitored. As the heart of the animal stopped beating, a rapid drop in OCV values was observed: in 10 min the OCV value settled at  $\sim 0.3$  V, which is almost 50% lower than the original OCV value. This can be attributed to the ceased flow of blood, and thereby depletion of  $O_2$  in the tissue surrounding the EFC. These measurements also confirm the bioelectrocatalytic origin of the electric power obtained from the implanted EFCs.

The typical electrochemical impedance (EI) values measured for EFCs in the brain, in CSF and buffer are presented in Fig. 8c. An ohmic resistance of about 5.5 k $\Omega$  in the brain tissue and in CSF was observed. EI values were also measured for EFCs in different buffer solutions (section 4 of SI, Fig. S9). The capacitance and the shape of impedance spectrum were found to be similar for EFCs in the brain and in CSF. However, the solution resistance along the electrodes was different, which can be attributed to the difference in the measurement conditions in the brain tissue and in the microcell. The main parameter here is the thickness of the electrolyte layer along the microelectrodes, the electrolyte layer along the microelectrodes inserted in the brain is narrow and consequently the solution resistance is higher.

Modelling of the EI data measured for implanted EFCs was performed with the equivalent circuit presented in the Fig. 8c inset. The data fit for the low frequency range (50 mHz–13 Hz) indicated that in this range the electric properties are mainly determined by the charge transfer resistance and the double layer capacitance ( $R_{ct}$  and  $C_{dl}$  in Fig. 8c, the inset)<sup>46</sup>. The data fit for the intermediate frequency range (13 Hz–7 kHz) indicated that in this range the electrical properties are mainly determined by the resistance of the distribution element impedance and the constant phase element ( $R_{p1}$  and  $CPE_{p1}$  in Fig. 8c, the inset), which was attributed to the distribution of electrical parameters along the electrodes and the depth of the porous layer. This is in a good agreement with theoretical prediction for highly porous electrodes<sup>47</sup>. The data fit for the high frequency range (7 kHz–40 kHz) indicated that in this range the electrical properties are mainly determined by the elements representing neurons ( $R_m$  and  $L_m$  in Fig. 8c, the inset), according to the theory developed by Hodgkin and Huxley (see detailed description in section 4 of SI, Fig. S10)<sup>48,49</sup>. Importantly, the inductive loop on the impedance spectrum appeared only when the EFCs were implanted in the brain (*cf.* curves 1–3 in Fig. 8c). We attributed this to the inductive properties of neuronal membranes, which contain voltage-gated ion channels that allow the neuron to generate and propagate an electrical signal by ion conduction<sup>49</sup>.

## Discussion

In the present study we show that the process underlying the simple method for fabrication of 3D nanostructured Au electrodes is, in all likelihood, based on an electrochemically driven transformation of physically deposited AuNPs into a genuinely 3D nanostructured material, in contrast to the previously suggested AuNPs aggregation



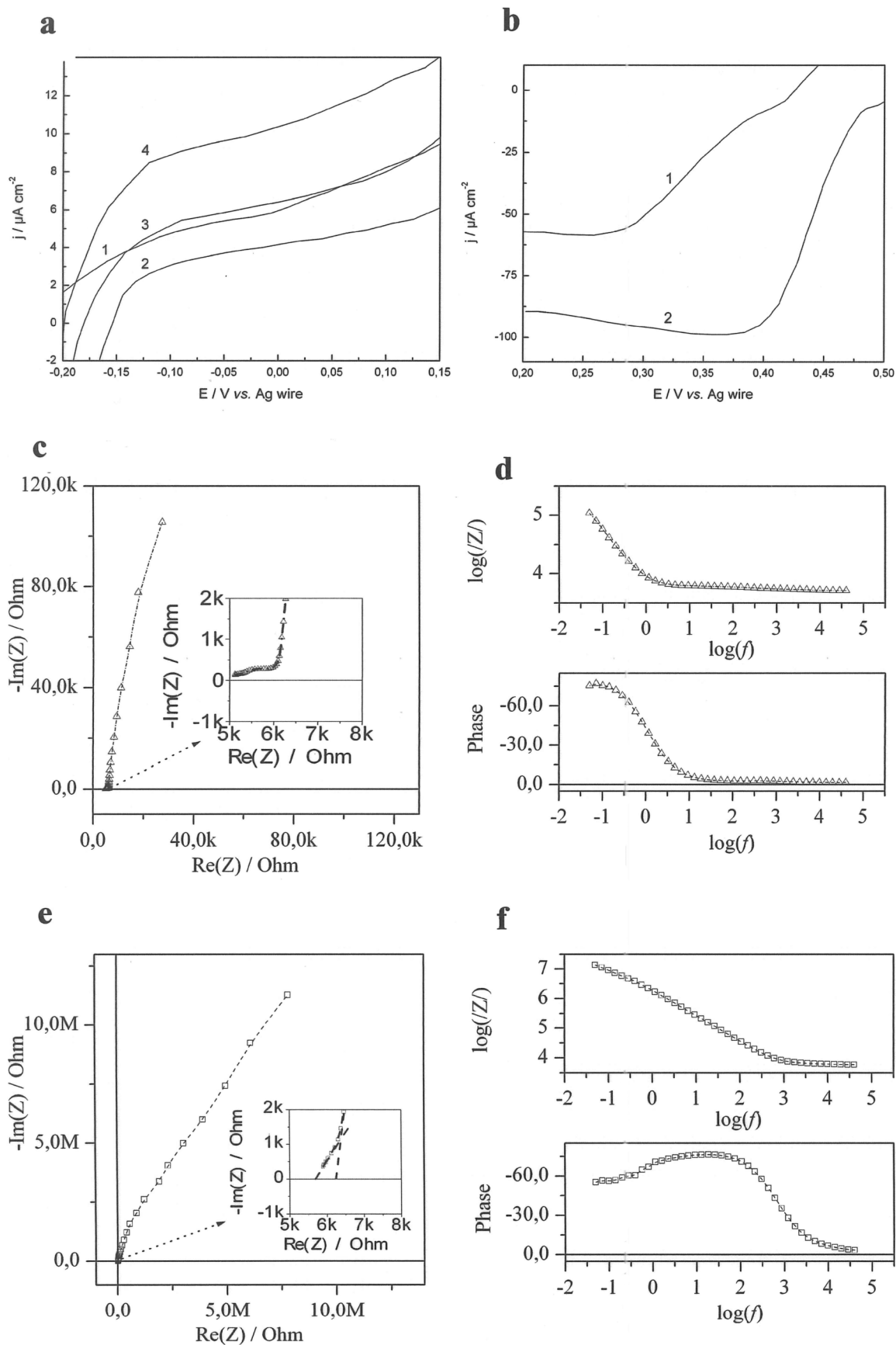


**Figure 6** | Electrochemical investigations of microelectrodes. (a) LSVs of microbioanode operating in CSF (1) and buffer containing 1 mM (2), 2.5 mM (3) and 5 mM glucose (4). (b) LSVs of microbioanode operating in CSF (1) and air saturated buffer containing 2.5 mM glucose (2); Conditions: 50 mM PBS, pH 7.4; scan rate  $0.3 \text{ mV s}^{-1}$ . (c) Nyquist plots and (d) Bode diagrams for AuNP modified Au microelectrodes in CSF. (e) Nyquist plots and (f) Bode diagrams for unmodified Au microelectrodes in CSF. Conditions for c,d,e,f:  $U = 0.45 \text{ V}$ ; amplitude = 10 mV.



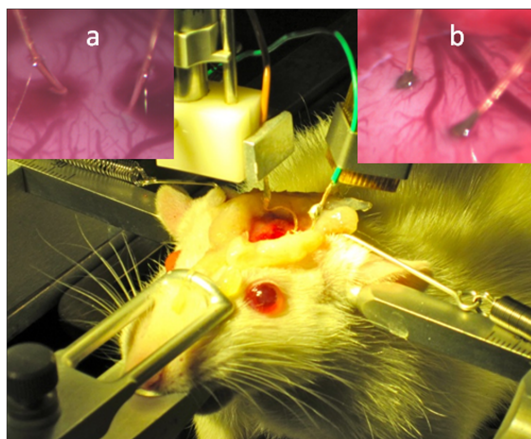


**Figure 7 | Enzymatic fuel cell implanted into the rat brain.** Photographs of the experimental arrangement for implantation of microbioelectrodes into the rat cortex, as well as close up pictures of the implantation with (a), and without (b), localised surface bleeding.

during solvent evaporation<sup>28</sup>. However, the underlying mechanism of this process is still unclear and calls for further investigations.

Using this process we fabricated 3D nanostructured electrically conducting microelectrodes with a geometric area increased 100 times. We confirmed that the geometrical area increase is indeed due to the formation of a genuinely 3D nanostructured Au surface. The electrochemical transformation of separate AuNPs into a solid nanostructured material with the formation of strong metallic bonds implies that 3D nanostructures fabricated with this simple method are mechanically robust, more sustainable in harsh conditions, and more biologically friendly compared to nanostructured materials made of physically agglomerated separate nanostructures. Formation of genuine and solid 3D Au nanostructure with an increase of the roughness factor<sup>28</sup> up to 300 times is remarkable and makes this type of material very desirable for neural prosthetics applications<sup>50</sup>. Moreover, the same simple approach can be employed for formation of complex nanostructures for different applications, and not necessarily only Au based materials. The finding reported here is also important for the electrochemical community, as the process exploited is commonly used for cleaning of Au electrode surfaces

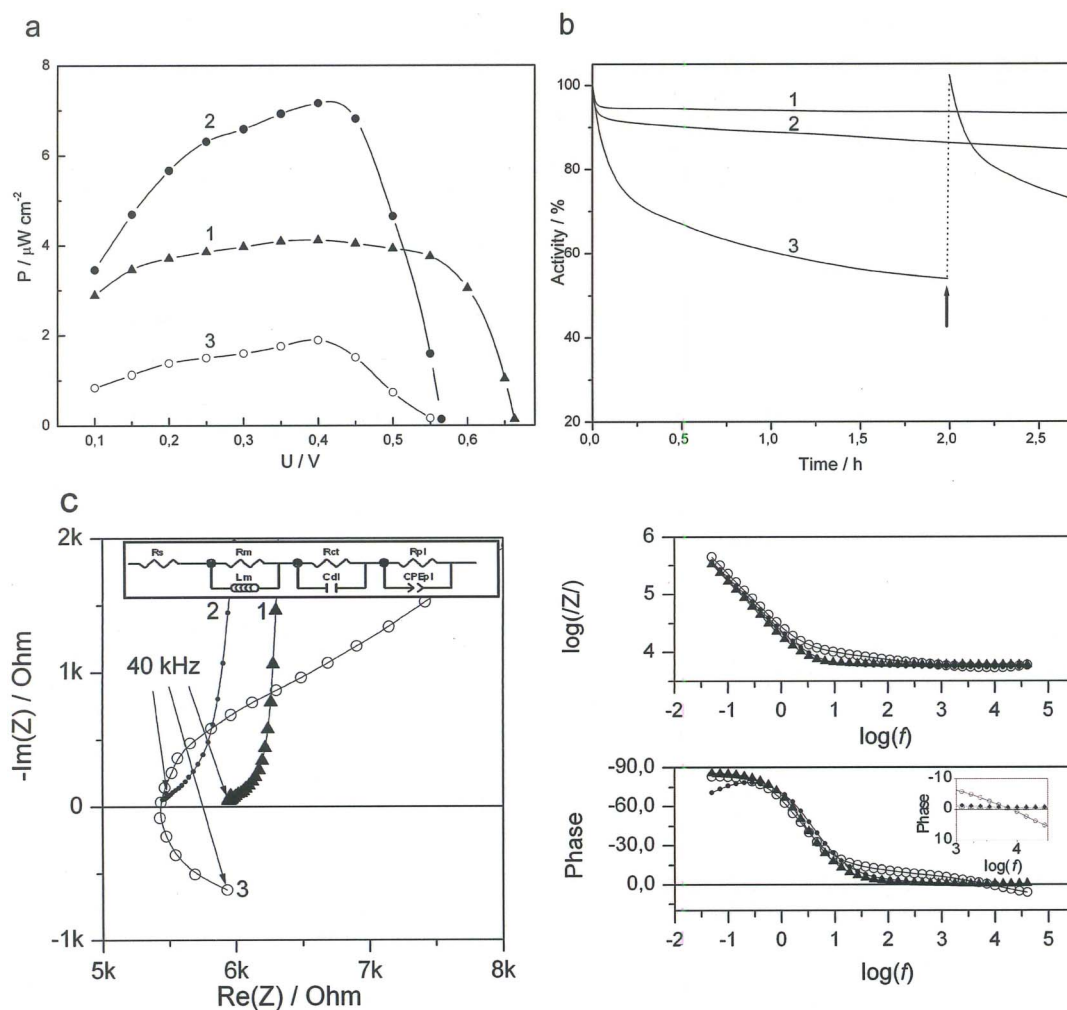


**Figure 8 | Enzymatic fuel cell characterisation.** (a) Typical power density plots of EFCs operating in buffer with 2.5 mM glucose (1), CSF (2), and rat brain (3). (b) Operational stability of EFCs operating in buffer with 2.5 mM glucose (1), CSF (2), and rat brain (3). At the time indicated by an arrow, a slight manipulation of the implanted electrodes was performed, moving them 0.1–0.2 mm. (c) Nyquist plots and Bode diagrams measured for EFCs in buffer (1, triangles), CSF (2, full circles), and rat brain (3, open circles). Insets: Equivalent circuit and magnified phase dependence.  $R_s$  – solution resistance,  $R_m$  – membrane resistance,  $R_{ct}$  – charge transfer resistance,  $R_{p1}$  – resistance of distribution element impedance,  $L_m$  – membrane inductivity,  $C_{dl}$  – double layer capacity,  $CPE_{p1}$  – constant phase element. Conditions: 50 mM PBS, pH 7.4; power density plots were obtained using both calibrated resistors of different resistance values and LSVs recorded with a scan rate of 0.3 mV s<sup>-1</sup>. The operational stability was measured at a constant load of 35.86 MΩ. Impedance measurements were done at  $U = 0.45$  V and an amplitude of 10 mV.



and also estimation of the effective (electrochemical or real) surface area. Until now this method has also been applied to nanostructured electrodes without the understanding that the process itself leads to the transformation of nanostructured Au surfaces.

We design 3D microbioanodes and microbioanodes by biomodification of 3D nanostructured Au electrodes with suitable bioelements, *viz.* *MvBOx* and *CtCDH*, respectively, and study the performance of nanobioelectrodes in CSF and in the rat brain. Prior to biomodification, the bioelements were thoroughly characterised in order to avoid any ambiguities regarding the results obtained. Combining a 3D microbioanode with a 3D microbioanode realises a mediator-, cofactor-, and membrane-less, microscale EFC. Owing to the simplicity of the design, substantial miniaturisation of the EFCs was possible, making the EFC implantation less traumatic and thus allowing adequate *in vivo* studies.

Only two reports exist on voltammetric studies of fully implantable EFCs operating *in vivo* in rats<sup>13–16</sup>. The basic parameters of the EFC detailed herein (OCVs, operating potentials, and power densities) are at least comparable, or even superior, to recently reported implanted biodevices (Table 1). However, the reported EFCs were macroscale and could not be used as low distress level EFCs operating in the brain.

Considering limitations, one could expect that the performance of the EFC designed by the combination of microbioanodes and microbioanodes, would be clearly limited by anodic bioelectrocatalytic reactions (*cf.* generated currents in Fig. 6a, b), at least when the EFC is operating *in vitro* using simple glucose containing solutions. Moving to physiological situations, *e.g.* from simple buffers to CSF, cathodes would definitely be responsible for a lowering of the voltage of the EFCs (*cf.* curves 1 and 2 in Fig. 6b) because of their depolarisation in CSF. Moreover, one could also expect significant decrease in current densities obtained from microbioanodes operating *in vivo*, because of the significantly lower concentration of available O<sub>2</sub> in both brain tissue and CSF in the living organism, *ca.* 50 μM<sup>51</sup>, compared to the air saturated solutions used in our *in vitro* studies, *ca.* 250 μM<sup>52</sup>. In the latter case, a decrease of the O<sub>2</sub> concentration from 250 to 50 μM resulted in a pronounced decrease of the bioelectrocatalytic currents (section 2 of SI, Fig. S7).

The obtained results unequivocally show an electric connection between nanostructured Au surfaces and neurons, evidenced by the appearance of inductive loops in the impedance spectra of bioelectrodes, a consequence of the inductive properties of neuronal membranes. This is a very interesting and practically applicable finding in the field of implantable nanostructure based neural interfaces, which is discussed in further detail in section 4 of SI. To the best of our knowledge, this is the very first impedance investigation of EFC-brain interfaces.

In summary, we present unequivocal experimental proof that microscale, mediator- and membrane-less EFCs do generate significant amounts of electrical energy for a self-powered biodevice, when operating in cerebrospinal fluid (*in vitro*) and when implanted in the rat brain (*in vivo*). To conclude, the present study shows without a doubt that miniature autonomous biodevices, *i.e.* wireless and self-powered biodevices, for minimally invasive neuron interfacing, which use nanostructured EFCs as electric power sources, are

practically realisable. This paves the road for a new generation of self-contained minimally invasive neural interfaces and brain-device applications.

## Methods

**Chemicals.** All chemicals were of analytical grade and used without further purification. All buffers were prepared with deionized water. 100 μm diameter Au wires and 130 μm silver wires were purchased from Goodfellow Cambridge Ltd. (Huntingdon, England).

AuNPs were prepared following a previously reported citrate-reduction procedure<sup>53</sup>. To concentrate the AuNPs, the AuNPs dispersion was centrifuged at 10000 × g for 30 min on a 5402 Eppendorf centrifuge (Eppendorf, Hamburg, Germany) in 1 mL Eppendorf tubes. Then, 98% of the supernatant was removed, the pelleted AuNPs were re-suspended by ultrasonication using an XB2 Ultrasonic Cleaner from VWR International Ltd. (East Grinstead, West Sussex, UK), and stored as a 50 times concentrated AuNPs dispersion at 4 °C.

*CtCDH* was obtained from a culture of *Corynebacterium thermophilus* CBS 405.69 (Centraalbureau voor Schimmelcultures, Utrecht, The Netherlands) and *MvBOx* was obtained as a kind gift from Amano Enzyme Inc. (Nagoya, Japan).

**Electrode fabrication.** 3D microbioanodes and microbioanodes were fabricated from Au microwires with a diameter of 100 μm. Firstly, wires were insulated using cellulose acetate (10 mg mL<sup>-1</sup>) dissolved in pure acetone. A section of roughly 3 mm was left un-insulated and used as a working surface. Secondly, electrodes were gently polished with 0.05 μm aluminium oxide powder (Struers A/S, Ballerup, Denmark), and cleaned electrochemically by cycling in the potential interval -0.2 V–1.7 V (*vs.* Ag/AgCl) for 20 cycles in 0.5 M H<sub>2</sub>SO<sub>4</sub>, with a scan rate of 100 mV s<sup>-1</sup>. Thirdly, several drops of concentrated AuNPs (*ca.* 1 μL) were applied to the surface of the cleaned electrodes, modifying roughly 1.5 mm of the working surface (projected [geometric] area of about 0.5 mm<sup>2</sup>). Thereafter, the electrodes were electrochemically cleaned again. The AuNPs-modified cathode was incubated in a 2 mg mL<sup>-1</sup> *MvBOx* solution for 2 h, washed with phosphate buffer saline (PBS) and was then ready for use. The AuNPs-modified anodes were incubated for 1 h in a mixed thiol solution (1 : 1 mixture of 1 mM 4-aminothiophenol and 1 mM 4-mercaptobenzoic acid), washed with ethanol, and incubated in *CtCDH* with glutaraldehyde as a crosslinker for 2 h (6 μL 23 mg mL<sup>-1</sup> CDH + 3 μL 2% glutaraldehyde). Finally, the anodes were carefully washed with PBS and were then ready for use.

A silver micro-reference electrode (Ag wire) was formed by cycling a silver microwire in the potential interval -0.5 V–0.5 V (*vs.* Ag/AgCl); 5 cycles in PBS. The thus obtained pseudo reference electrode had a potential of about 270 mV (*vs.* NHE) in PBS.

For heterogeneous activity measurements, macroscale Au rotating disk electrodes (RDEs) (Bioanalytical Systems, West Lafayette, IN, USA) were prepared following a procedure similar to the assembly of microbioelectrodes.

**Animal handling and implantation.** A total of 4 adult female Sprague Dawley rats weighing 260–320 g were used. The animals received food and water *ad libitum*, and were kept in a 12-h day-night cycle at a constant environmental temperature of 21 °C (rel. humidity 65%). Approval for the experiments was obtained in advance from the Lund/Malmö local ethical committee on animal experiments, regulated by the code of regulations of the Swedish Board of Agriculture. These regulations, including directives from the European Union, follow the law on animal welfare legislated by the Swedish parliament. The County Administrative Board governs the implementation of the rules. Further, the experiments were in accordance with the policies and guidelines reported previously<sup>54</sup>.

The rats were anaesthetised *via* intraperitoneal injections with a mixture (20 : 1, 6.3 ml kg<sup>-1</sup>) of Fentanyl Citrate (Fentanyl, B Braun, Melsungen Germany) and Medetomidine (Domitor, Orion Pharma, Espoo Finland) and attached to a stereotaxic frame for the duration of the experiment. To measure electrode performance, the cortex surface (4–5 mm<sup>2</sup>) was exposed with a craniotomy followed by removal of the dura. Care was taken to keep the brain surface moist with 0.9% saline solution, to prevent drying of the brain.

The electrode probes were attached to micromanipulators, allowing slow and controllable insertion during implantation, and electrically connected to a potentiostat. The implantations were made under visual inspection using a microscope to a maximum depth of approximately 2 mm. In a separate set of experiments, an incision

**Table 1** | Comparison of basic characteristics of EFCs implanted in rats. EFCs recently detailed in Refs. 15, 16 were built from carbon nanotubes (CNTs) and buckypaper (BP) using glucose oxygen (GOx) or glucose dehydrogenase (GDH) as anodic and laccase (Lc) as cathodic bioelements, respectively

Anode/Cathode	OCV (V)	Power (μW cm <sup>-2</sup> )	Operating Voltage (V)	Reference
GOx-CNTs/Lc-CNTs	0.57	195	<i>ca.</i> 0.4*	Zebda et al. <sup>16</sup>
GDH-BP/Lc-BP	0.14	<5	<0.1	Castorena-Gonzalez et al. <sup>15</sup>
CDH-AuNPs/BOx-AuNPs	0.54	2	0.4	Present study

Note: \* - voltage was re-calculated from Fig. 2C in Ref. 16.



was made between the skull and the first cervical vertebra. CSF was carefully drained through a small hole in the dura matter by aid of a glass pipette. The CSF was centrifuged at  $10000 \times g$  at  $4^\circ\text{C}$  for 20 min and the supernatant was used for electrochemical characterisation of electrodes. After the experiments, each rat was sacrificed by a lethal dose of Sodium Pentobarbital (Apoteket, Sweden).

**Activity measurements.** The activity of *MvBOx* was determined using 5 mM  $\text{K}_4[\text{Fe}(\text{CN})_6]$  solutions at different pH; the activity was assessed using an Anthelie Advanced Spectrophotometer (Topac Inc., Cohasset, MA, USA). When immobilised on RDEs, the *MvBOx* activity was assessed using a BASi RDE-2 system (Bioanalytical Systems, West Lafayette, IN, USA) with a rotation rate of 2000 rpm. Similarly, the activity of *CtCDH* was determined in 20  $\mu\text{M}$  cytochrome *c* solutions at different pH, also when immobilised on RDEs.

**Electrochemical investigations. Electrochemical measurements.** Electrochemical measurements were carried out using a  $\mu\text{Autolab}$  Type III/FRA2 potentiostat/galvanostat from Metrohm Autolab B.V. (Utrecht, The Netherlands). Electrochemical impedance was measured with a voltage amplitude perturbation of 5 mV using a 50 kHz–10 mHz frequency range. Fitting of the impedance data was done using the ZView 2.0 programme from ZView 2.80, from Scribner Associates Inc. (Southern Pines, NC, USA), in the frequency interval 1 kHz to 10 mHz. Unless otherwise noted, all *in vitro* characterisations were performed in a microcell made from a glass capillary with a volume of roughly 15  $\mu\text{L}$  and an internal diameter of 1.5 mm.

The electrodes were characterised individually in PBS, pH 7.4, with different glucose concentrations as well as in CSF using the Ag wire reference electrode as a combined counter and reference electrode. The microbioelectrodes were evaluated by LSV using a scan rate of  $0.3 \text{ mV s}^{-1}$ . Basic EFC parameters were evaluated in PBS, CSF, and *in vivo* in the brain, and obtained using the anode as the working electrode and the cathode as a combined counter/reference electrode, without any separating membrane. The performance was evaluated by LSV, changing the voltage with a scan rate of  $0.3 \text{ mV s}^{-1}$  from the OCV to lower voltage regions, while recording the current in the circuit. The low scan rate eliminated charging currents of the double layer. As a complementary method to characterize the EFC performance, measurements were performed with different calibrated resistors, 1–100 M $\Omega$ , from Velleman Inc. (Forth Worth, TX, USA). The resistors were calibrated using a  $\mu\text{Autolab}$  Type III/FRA2, input impedance  $>100 \text{ G}\Omega$ . The system was allowed 3 min to reach equilibrium for each point. The stability of the EFC was determined by monitoring the change in voltage, when a constant load of 35.86 M $\Omega$  was applied to the EFC.

**Verification of electrochemical measurements.** About 100 bioelectrodes in total were fabricated during our studies. Averaged OCV and power density values are based on at least three measurements *in vitro*. Typical plots showing *in vitro* studies were calculated averaging the results from at least three different measurements. Four different animals were used in our *in vivo* studies. Thus, averaged OCV and power density values are based on four different measurements *in vivo*. Typical plots showing *in vivo* studies were calculated by averaging the results from two different measurements. Importantly, no significant differences were observed, when actual steady-state measurements were used to evaluate the performance of EFCs, compared to LSVs measurements at low scan rates.

**AFM and SEM studies.** AFM images of the nanoscopic surfaces were obtained using a Multimode VIII SPM with a Nanoscope V control unit (Bruker AXS, Santa Barbara, CA, USA). The AFM was operated in the ScanAsyst mode. All images were obtained in air and at room temperature. Triangular silicon nitride cantilevers with a nominal spring constant of  $0.4 \text{ N m}^{-1}$  (ScanAsyst Air probes, Bruker AXS) were employed in all measurements. Analysis and processing of AFM images was performed with the WSxM software package<sup>55</sup>. Image processing consisted of plane subtraction, equalization and 3D representation.

Poly-L-lysine (PL) coated mica sheets (Electron Microscopy Sciences, Hatfield, PA, USA) were used as a substrate for the visualization of single AuNPs. Coating was done by pipetting a 10  $\mu\text{L}$  PL (aqueous solution 0.01% w/w) drop onto a freshly cleaved mica sheet in order to provide a positively charged surface on which the negatively charged AuNPs would adsorb. After incubation for 30 sec, the surface was gently rinsed with UHQ water and dried in a nitrogen stream, to ensure that only strongly adsorbed PL chains remained on the surface. Afterwards, the surface was incubated in a AuNPs suspension for 1 min, then rinsed with UHQ water, and dried in a  $\text{N}_2$  stream before being placed in the microscope.

SEM images were obtained using a high resolution SEM FEI Nova NanoLab 600 in field immersion mode at 15 kV accelerating voltage and 36 pA beam current. The reference samples for original AuNPs visualisation with SEM were made of silicon wafers covered with 2000 Å of Au film on top of 25 Å titanium adhesion layer, the deposition was done in a Balzers UMS 500 P system (Balzers, Neugrüt, Lichtenstein) by electron-beam evaporation. The AuNPs coating was done by pipetting of 5  $\mu\text{L}$  of AuNPs suspension and drying in air.

- Kipke, D. R. *et al.* Advanced neurotechnologies for chronic neural interfaces: new horizons and clinical opportunities. *J. Neurosci.* **28**, 11830–11838 (2008).
- Kotov, N. A. *et al.* Nanomaterials for neural interfaces. *Adv. Mater.* **21**, 3970–4004 (2009).

- Vaadia, E. & Birbaumer, N. Grand challenges of brain computer interfaces in the years to come. *Front. Neurosci.* **3**, 151–154 (2009).
- Cohen-Karni, T., Langer, R. & Kohane, D. S. The smartest materials: The future of nanoelectronics in medicine. *ACS Nano* **6**, 6541–6545 (2012).
- Schouenborg, J. Biocompatible multichannel electrodes for long-term neurophysiological studies and clinical therapy--novel concepts and design. *Prog. Brain Res.* **194**, 61–70 (2011).
- Bryllert, T., Wernersson, L.-E., Froeberg, L. E. & Samuelson, L. Vertical high-mobility wrap-gated InAs nanowire transistor. *IEEE Electron Device Lett.* **27**, 323–325 (2006).
- Lieber, C. M. Semiconductor nanowires: a platform for nanoscience and nanotechnology. *MRS Bull.* **36**, 1052–1063 (2011).
- Svensson, C. P. T. *et al.* Monolithic GaAs/InGaP nanowire light emitting diodes on silicon. *Nanotechnology* **19**, 305201/305201–305201/305206 (2008).
- Suyatin, D. B. *et al.* Nanowire-based electrode for acute *in vivo* neural recordings in the brain. *PLoS One* **8**, e56673 (2013).
- Barton, S. C., Galloway, J. & Atanassov, P. Enzymatic biofuel cells for implantable and microscale devices. *Chem. Rev.* **104**, 4867–4886 (2004).
- Freguia, S., Viridis, B., Harnisch, F. & Keller, J. Bioelectrochemical systems: Microbial versus enzymatic catalysis. *Electrochim. Acta* **82**, 165–174 (2012).
- Rapoport, B. I., Kedzierski, J. T. & Sarpeshkar, R. A glucose fuel cell for implantable brain-machine interfaces. *PLoS One* **7**, e38436 (2012).
- Cinquin, P. *et al.* A glucose biofuel cell implanted in rats. *PLoS One* **5**, e10476 (2010).
- Miyake, T. *et al.* Enzymatic biofuel cells designed for direct power generation from biofluids in living organisms. *Energy Environ. Sci.* **4**, 5008–5012 (2011).
- Castorena-Gonzalez, J. A. *et al.* Biofuel cell operating *in vivo* in rat. *Electroanalysis* **25**, 1579–1584 (2013).
- Zebda, A. *et al.* Single glucose biofuel cells implanted in rats power electronic devices. *Sci. Rep.* **3**, 1516, DOI:10.1038/srep01516 (2013).
- Falk, M., Narvaez Villarrubia, C. W., Babanova, S., Atanassov, P. & Shleev, S. Biofuel cells for biomedical applications: colonizing the animal kingdom. *ChemPhysChem* **14**, 2045–2058 (2013).
- Shleev, S. *et al.* High-performance, size-optimized, nanostructure-based biofuel cell operating in rat brain. *63rd Annual ISE Meeting*, August 19–24, Czech Republic, (2012).
- Falk, M. *et al.* *In vivo* operating miniature, direct electron transfer based, membrane-less glucose/oxygen biofuel cell in rat brain. *222<sup>nd</sup> ECS Meeting*, October 7–12, Hawaii, (2012).
- Minteer, S. D. Nanobioelectrocatalysis and its applications in biosensors, biofuel cells and bioprocessing. *Top. Catal.* **55**, 1157–1161 (2012).
- Tamaki, T. Enzymatic biofuel cells based on three-dimensional conducting electrode matrices. *Top. Catal.* **55**, 1162–1180 (2012).
- Falk, M., Blum, Z. & Shleev, S. Direct electron transfer based enzymatic fuel cells. *Electrochim. Acta* **82**, 191–202 (2012).
- Coman, V. *et al.* A direct electron transfer-based glucose/oxygen biofuel cell operating in human serum. *Fuel Cells* **10**, 9–16 (2010).
- Coman, V. *et al.* A membrane-, mediator-, cofactor-less glucose/oxygen biofuel cell. *Phys. Chem. Chem. Phys.* **10**, 6093–6096 (2008).
- Pan, C. *et al.* Generating electricity from biofluid with a nanowire-based biofuel cell for self-powered nanodevices. *Adv. Mater.* **22**, 5388–5392 (2010).
- Wang, X. *et al.* Mediatorless sugar/oxygen enzymatic fuel cells based on gold nanoparticle-modified electrodes. *Biosens. Bioelectron.* **31**, 219–225 (2012).
- Falk, M. *et al.* Biofuel cell as a power source for electronic contact lenses. *Biosens. Bioelectron.* **37**, 38–45 (2012).
- Murata, K. *et al.* A simple fabrication method for three-dimensional gold nanoparticle electrodes and their application to the study of the direct electrochemistry of cytochrome *c*. *Electroanalysis* **22**, 185–190 (2010).
- Murata, K., Kajiya, K., Nakamura, N. & Ohno, H. Direct electrochemistry of bilirubin oxidase on three-dimensional gold nanoparticle electrodes and its application in a biofuel cell. *Energy Environ. Sci.* **2**, 1280–1285 (2009).
- Dagys, M. *et al.* Laccase-gold nanoparticle assisted bioelectrocatalytic reduction of oxygen. *Electrochem. Commun.* **12**, 933–935 (2010).
- Trasatti, S. & Petrii, O. A. Real surface area measurements in electrochemistry. *Pure Appl. Chem.* **63**, 711–734 (1991).
- Chesler, M. Regulation and modulation of pH in the brain. *Physiol. Rev.* **83**, 1183–1221 (2003).
- Rehncrona, S. Brain acidosis. *Ann. Emerg. Med.* **14**, 770–776 (1985).
- Ludwig, R., Harreither, W., Tasca, F. & Gorton, L. Cellobiose dehydrogenase: A versatile catalyst for electrochemical applications. *ChemPhysChem* **11**, 2674–2697 (2010).
- Shleev, S. *et al.* On the possibility of uphill Intramolecular electron transfer in multicopper oxidases: electrochemical and quantum chemical study of bilirubin oxidase. *Electroanalysis* **24**, 1524–1540 (2012).
- Sherwood, L. *Human physiology: from cells to systems*. 558–569 (Brooks/Cole, Pacific Grove, 2001).
- Mak, W., Cheng, T. S., Chan, K. H., Cheung, R. T. F. & Ho, S. L. Cerebrospinal fluid to serum glucose ratio in non-hypoglycemic neurological conditions. *Hong Kong Med. J.* **11**, 457–462 (2005).
- Reiber, H., Ruff, M. & Uhr, M. Ascorbate concentration in human cerebrospinal fluid (CSF) and serum. Intrathecal accumulation and CSF flow rate. *Clin. Chim. Acta* **217**, 163–173 (1993).





39. Shaidarova, L. G., Chelnokova, I. A., Romanova, E. I., Gedmina, A. V. & Budnikov, G. K. Joint voltammetric determination of dopamine and uric acid. *Russ. J. Appl. Chem.* **84**, 218–224 (2011).
40. Vidakovic-Koch, T. *et al.* Impact of the gold support on the electrocatalytic oxidation of sugars at enzyme-modified electrodes. *Electroanalysis* **23**, 927–930 (2011).
41. Teng, H., Liu, Y. & You, T.-Y. Facile synthesis of gold nanoparticle-loaded carbon nanofiber composites and their electrocatalytic activity towards dopamine, ascorbic acid and uric acid. *Chem. Res. Chin. Univ.* **27**, 496–499 (2011).
42. Bayir, H. *et al.* Assessment of antioxidant reserves and oxidative stress in cerebrospinal fluid after severe traumatic brain injury in infants and children. *Pediatr. Res.* **51**, 571–578 (2002).
43. Hall, J. E. & Guyton, A. C. *Textbook of medical physiology*. 562–564 (Saunders/Elsevier, Philadelphia, 2011).
44. Agus, D. B. *et al.* Vitamin C crosses the blood-brain barrier in the oxidized form through the glucose transporters. *J. Clin. Invest.* **100**, 2842–2848 (1997).
45. Sun, F. *et al.* Change in tissue concentrations of lipid hydroperoxides, vitamin C and vitamin E in rats with streptozotocin-induced diabetes. *Clin. Sci.* **96**, 185–190 (1999).
46. Lasia, A. Electrochemical impedance spectroscopy and its applications. *Mod. Aspects Electrochem.* **32**, 143–248 (1999).
47. Aurbach, D., Levi, M. D. & Levi, E. A review on the solid-state ionics of electrochemical intercalation processes: How to interpret properly their electrochemical response. *Solid State Ionics* **179**, 742–751 (2008).
48. Hodgkin, A. L. & Huxley, A. F. A quantitative description of membrane current and its application to conduction and excitation in nerve. *J. Physiol.* **117**, 500–544 (1952).
49. Magee, J. Voltage-gated ion channels in dendrites. *Dendrites*. Stuart, G., Spruston, N., Hausser, M. (eds.) 139–160 (Oxford University Press, New York, 1999).
50. Zhang, H., Shih, J., Zhu, J. & Kotov, N. A. Layered nanocomposites from gold nanoparticles for neural prosthetic devices. *Nano Lett.* **12**, 3391–3398. doi:10.1021/nl3015632 (2012).
51. Bazzu, G. *et al.* Real-time monitoring of brain tissue oxygen using a miniaturized biotelemetric device implanted in freely moving rats. *Anal. Chem.* **81**, 2235–2241 (2009).
52. Truesdale, G. A. & Downing, A. L. Solubility of oxygen in water. *Nature* **173**, 1236 (1954).
53. Frens, G. Controlled nucleation for the regulation of the particle size in monodisperse gold suspensions. *Nature, Phys. Sci.* **241**, 20–22 (1973).
54. Drummond, G. B. Reporting ethical matters in The Journal of Physiology: standards and advice. *J. Physiol.* **587**, 713–719 (2009).
55. Horcas, I. *et al.* WSXM: a software for scanning probe microscopy and a tool for nanotechnology. *Rev. Sci. Instrum.* **78**, 013705/013701–013705/013708 (2007).
56. Fromherz, P. Electrical interfacing of nerve cells and semiconductor chips. *ChemPhysChem* **3**, 276–284 (2002).
57. Keller, D. Reconstruction of STM and AFM images distorted by finite-size tips. *Surf. Sci.* **253**, 353–364 (1991).

## Acknowledgments

The authors thank Amano Enzyme Inc. for a kind gift of Amano 3 preparation. The authors would like to acknowledge also D. Csontos for helpful suggestions and fruitful discussions. The work has been supported financially by the Swedish Research Council (2013-6006), Linnaeus grant (80658701), the Knut and Alice Wallenberg Foundation (KAW 2004.0119), the Nanometer Structure Consortium at Lund University (nmC@LU), and by the Russian Foundation for Basic Research (12-04-33102 and 13-04-12083).

## Author contributions

S.S., D.B.S., V.O.P., Z.B., and Je.Sc. conceived and initiated the project. S.S. conceived and supervised the experiments. V.A. and M.F. prepared and electrochemically characterised EFCs. Ja.So. and D.B.S. performed AFM and SEM studies, respectively, and analysed the data. S.S., Je.Sc., M.G. D.B.S., V.A., and M.F. performed *in vivo* experiments. M.G. and Je.Sc. obtained ethical approval for experiments. R.L. isolated, purified, and characterised bioelements. S.S., Z.B., Je.Sc., D.B.S., and V.O.P. wrote the manuscript. All authors discussed the results and implications, and commented on the work.

## Additional information

**Supplementary information** accompanies this paper at <http://www.nature.com/scientificreports>

**Competing financial interests:** The authors declare no competing financial interests.

**How to cite this article:** Andoralov, V. *et al.* Biofuel Cell Based on Microscale Nanostructured Electrodes with Inductive Coupling to Rat Brain Neurons. *Sci. Rep.* **3**, 3270; DOI:10.1038/srep03270 (2013).



This work is licensed under a Creative Commons Attribution-NonCommercial-NoDerivs 3.0 Unported license. To view a copy of this license, visit <http://creativecommons.org/licenses/by-nc-nd/3.0>